PALEOCEANOGRAPHY, VOL. ???, XXXX, DOI:10.1029/,

Organic Carbon Burial following the Middle Eocene Climatic Optimum (MECO) in the central - western Tethys

D.J.A. Spofforth[1], C. Agnini[2], H. Pälike[1], D. Rio[2], E. Fornaciari[2], L. Giusberti[2], V. Luciani[3], L. Lanci[4], G. Muttoni[5]

(1) School of Ocean and Earth Science, University of Southampton, UK

(2) Department of Geosciences, University of Padua, Italy

(3) Department of Earth Sciences, University of Ferrara, Italy

(4) Instituto di Dinamica Ambientale, University of Urbino, Italy

(5) Department of Earth Sciences, University of Milano, Italy

David JA Spofforth & Heiko Pälike, University of Southampton, School of Ocean and Earth Science, European Way, Southampton, SO14 3ZH, U.K. (djas@noc.soton.ac.uk, heiko.palike@noc.soton.ac.uk).

Abstract

We present trace metal geochemistry and stable isotope records for the middle Eocene Alano di Piave section, NE Italy, deposited during magnetochron C18n in the marginal Tethys Ocean. We identify a $\sim$ 500 kyr long carbon isotope perturbation event we infer to be the middle Eocene Climatic Optimum (MECO) confirming the northern hemisphere expression and global occurrence of MECO. Interpreted peak climatic conditions are followed by the rapid deposition of two organic rich intervals ($\leq$3% TOC) and contemporaneous positive δ^{13}C excursions. These two intervals are associated with increases in the concentration of sulphur and redox-sensitive trace metals, and low concentrations of Mn, as well as coupled with the occurrence of pyrite. Together these changes imply low, possibly dysoxic, bottom water O_2 conditions promoting increased organic carbon burial. We hypothesize that this rapid burial of organic carbon lowered global pCO_2 following the peak warming and returned the climate system to the general Eocene cooling trend.

1. Introduction

Peak Cenozoic warmth during the Early Eocene Climatic Optimum (~50 - 52 Ma) [*Zachos et al.*, 2001] was followed by gradually cooling temperatures through the Eocene with the development of permanent ice-sheets on Antarctica around the Eocene-Oligocene boundary (~33.8 Ma) [*Zachos et al.*, 1996; *Coxall et al.*, 2005; *Lear et al.*, 2008]. This long term cooling has been mostly attributed to decreased atmospheric $p\mathrm{CO}_2$ and its feedbacks within the climate system [*Raymo*, 1991; *Berner and Kothavala*, 2001; *DeConto and Pollard*, 2003; *Pagani et al.*, 2005; *Liu et al.*, 2009]. Reconstructions of past Cenozoic $p\mathrm{CO}_2$ suggest concentrations decreased stepwise from 1000 - 1500 ppmV in the middle - late Eocene to near modern day values by the late Oligocene [*Pagani et al.*, 2005].

Superimposed on the Eocene long term cooling trend are a series of transient positive and negative oxygen isotope excursions interpreted as warming [*Bohaty and Zachos*, 2003; *Sexton et al.*, 2006; *Edgar et al.*, 2007b; *Ivany et al.*, 2008; *Bohaty et al.*, 2009] and cooling and/or glaciation events [*Tripati et al.*, 2005; *Edgar et al.*, 2007b]. Climate model results for the Eocene Antarctic run under several possible pCO_2 conditions indicate that small ephemeral ice sheets may have been possible under weak greenhouse conditions [*DeConto and Pollard*, 2003; *DeConto et al.*, 2008] and even small ice caps at elevated regions were possible under higher pCO_2 with favorable orbital configurations. Similarly, prominent changes in the calcium compensation depth in the equatorial Pacific [*Rea and Lyle*, 2005] further suggest that the middle Eocene experienced large changes within the global carbon cycle.

Short lived negative δ^{13}C excursions punctuate the Eocene [*Cramer et al.*, 2003; *Lourens et al.*, 2005; *Sexton et al.*, 2006; *Nicolo et al.*, 2007; *Edgar et al.*, 2007b]. Some of these have previously been inferred to represent short-lived warming events e.g. [*Sluijs et al.*, 2008a, b]. However, at least one longer transient warming event is recorded during the Eocene [*Bohaty and Zachos*, 2003; *Bohaty et al.*, 2009]. During the middle Eocene climatic optimum (MECO) [*Bohaty and Zachos*, 2003; *Bohaty et al.*, 2009] Southern Ocean deep water temperatures warmed by up to 4°C and lasted for $\sim$ 500 kyrs before rapidly cooling. Recent identification of a positive δ^{13}C anomaly in the Tethys [*Jovane et al.*, 2007] has been tentatively correlated to the MECO event, and confirmed by new dating of the original sites [*Bohaty et al.*, 2009], suggesting a global occurrence of this event.

On timescales of several hundred thousand years chemical weathering of silicate rocks and the rate of volcanic gas emissions control pCO$_2$ concentrations, but shorter timescale variations require different mechanisms. The Paleocene – Eocene thermal maximum (PETM), for example, is frequently explained by rapid ($< 10^4$ yr [*Zachos et al.*, 2005]) release and oxidation of CH$_4$ clathrates to pCO$_2$ [*Dickens et al.*, 1995; *Thomas et al.*, 2002] leading to 4 - 5°C deep sea [*Kennett and Stott*, 1991; *Zachos et al.*, 2001] and 5 - 8°C of global surface warming [*Zachos et al.*, 2003; *Sluijs et al.*, 2006, 2008a]. Similarly rapid decreases in pCO$_2$ can also occur through increased productivity and/or increased rates of organic carbon burial [*John et al.*, 2008] on similar time scales, as well as changes in chemical weathering rates of terrestrial carbonates [*Archer et al.*, 1998; *Ridgwell and Hargreaves*, 2007; *Stap et al.*, 2009].

Here we identify the northern hemisphere occurrence and confirm the timing of MECO from a site in the central-western Tethys. High resolution bulk sediment stable isotope and percentage $CaCO_3$ studies are coupled with bulk sediment geochemistry and kerogen analysis to investigate paleoenvironmental responses to this climatic perturbation. We report previously unrecorded locally low bottom water oxygen saturation following the main excursion of the event. We suggest that high organic carbon burial immediately following MECO is the most likely mechanism for reduction in $p\mathrm{CO}_2$ and the return to the general cooling trend.

2. Methods

2.1. Materials

The middle/late Eocene Alano di Piave section outcrops in the Belluno Basin in the Southern Alps of NE Italy (Figure 1). Comprising part of the middle Eocene - upper Eocene Marna Scagliosa di Alano formation [*Agnini et al.*, (in press) 2009], this section outcrops along the Calcino Creek close to Alano di Piave village (Latitude 45°54'50"N, Longitude 11°54'55"E). The lithology consists mainly of bathyal grey marls, with occasional indurated limestones beds. This formation outcrops for $\sim$ 110m stratigraphic thickness and was deposited in middle-upper bathyal water depths (L.Giusberti. unpubl. data). Paleoenvironmental reconstructions (Figure 1A,C) of the Tethys region [*Dercourt et al.*, 1993; *Smith et al.*, 1994; *Scotese*, 2002; *Bosellini and Papazzoni*, 2003] suggest that the climate was predominately sub-tropical and that the Alano section was deposited to the east of a carbonate platform and within $\sim 100 - 150$ km of land.

Sediment samples were collected at each lithological change or every 20 cm if individual beds were thicker than this. The average sample spacing for all samples was $\sim$ 20cm. During sample collection all weathered material was removed. In this study we particularly focus on a darker organic rich interval $\sim$ 17-25 m down the river valley from where rocks first outcrop.

Stratigraphically the interval from 17 - 25 m is characterized by dark colored marls with rare sub-cm scale clay horizons, increases in the amount of pyrite and occasional laminated sediments. The top of the interval is marked by a coarse calcareous arenite, the Palladio Bed, overlain by a $\sim$ 20 cm thick low $CaCO_3$ clay layer before a return to more marly deposition. The dark colored interval is split into 2 units by a lighter colored interval from $\sim$ 19 - 21 m.

Geochemical, magnetic and biostratigraphic data were obtained using standard methods for the entire Alano section (see supplementary information).

3. Results

3.1. Magnetobiostratigraphic framework

The Alano di Piave section extends from calcareous nannofossil zone NP16 to zone NP19-20 [*Martini*, 1971], and from planktonic foraminiferal zone E10-E11 to zone E15 [*Berggren and Pearson*, 2005]. Magnetostratigraphic data indicates that this section was deposited between the upper part of magnetochron C18r and the very base of chron C16r [*Cande and Kent*, 1995]. The present biochronology available for the middle to late Eocene interval is based on a limited dataset in *Berggren et al.* [1995]. The age estimates obtained for first, last and peak occurrences of biostratigraphic markers from the Alano section based on linear sedimentation rates applied to the magnetostratigraphy *Pälike et al.* [2006a], differ from those presented in *Berggren et al.* [1995]. They are, however, consistent with calibrations obtained for calcareous nannofossil and planktonic foraminifera from Blake Nose (ODP Site 1052) [*Wade*, 2004]. The age model (Figure S1) developed by us (supplementary information) and applied here, relies on the magnetostratigraphic framework and dates this section from the top of chron C18r to the base of chron C16r (40.96 - 36.50 Ma using the *Pälike et al.* [2006a] timescale). Additionally, as recorded in Contessa [*Jovane et al.*, 2007] and at ODP Site 1051 [*Edgar et al.*, 2007a] the first occurence of the key biostratigraphic datum *Orbulinoides beckmanni* coincides, here at Alano, with the onset of MECO confirming the magnetostratigraphic placement of the event.

3.2. Bulk δ^{13}C and δ^{18}O Isotope Data

Isotope results from the Alano section are shown in Figure 2. These show a gradual decrease of ~ 0.5‰ in both δ^{13}C and δ^{18}O up section. The $CaCO_3$ content also decreases from $\sim 50\%$ to $\sim 45\%$ over the same interval. Superimposed on this overall trend is a prominent transient isotope excursion beginning at ~13 m (Figure 3). Bulk δ^{18}O records a negative shift of up to -1.8 ‰ with the minimum δ^{18}O values (labeled A in Figure 3) at $\sim$ 17 m, coincident with the beginning of the first darker unit and representing the peak of the event. Similarly δ^{13}C and $CaCO_3$ record minimum values of 0.2 ‰ (from $\sim$ 1‰) and 20% (from 50%) respectively. Although the δ^{18}O record gradually recovers to near-pre-event values by 25 m, the δ^{13}C and $CaCO_3$ records are more complex (Figure 3) and are strongly correlated to the observed lithological changes. Two rapid positive δ^{13}C excursions (labeled B and D) are interrupted by a negative excursion to near peak event values at ∼ 19 - 21 m (labeled C). The two positive carbon isotope excursions are similar in magnitude (1.25 ‰) and are coincident with elevated organic carbon content (up to 3%)(Figure 3). At the beginning of the first darker interval the $CaCO_3$ recovers to maximum values occurring in the 19 - 21 m interval. A small decrease (∼ 5%) is recorded during the positive δ^{13}C excursion during the second organic rich layer.

3.3. Organic Carbon

Two organic rich units are recognised (from here on referred to as ORG1 and ORG2) and are recorded in TOC data (Figure 3). Pre-event and post-event values are low around 0.1 - 0.15 % rising to a peak of 3.1 % between 16.8 and 19 m and 21 - 25.5 m, respectively. Within each organic rich unit the amount of TOC present is not constant but appears to vary cyclically (Figure 3). In particular, ORG2 between 20.9 - 25.5 m has 4 prominent peaks in organic carbon content, ∼ 1.4 m apart. The major component of organic carbon in these intervals is marine amorphous organic matter, although minor amounts of wood, pollen, fungal spores, dinocysts and rare benthic foraminifer linings are also present.

$\delta^{13}C_{org}$ analysis of organic material (Figure 3) follows the same trend and pattern as the TOC data. Negative isotope excursions of ∼ 1‰ occur within both organic rich intervals. The initial excursion leads the TOC increase by ∼ 40 cm in ORG1 while the shift associated with ORG2 has occurred by ∼ 21.5 m, coincident with the second TOC spike. The ORG2 data is ambiguous as to whether δ^{13}C$_{org}$ leads or lags the TOC data.

3.4. Bulk Sediment Geochemistry

3.4.1. $CaCO_3$, TOC and Detrital inputs

Immediately following the maximum negative carbon isotope excursion there are strong lithological indicators in the form of organic rich dark shales and clay layers that there were variations in the paleoceanographic conditions at this time. Assuming the Si content of the sediment to be of detrital origin, the slope of the Al-Si plot (Figure S2) shows an average shale value of ~ 3, we assume that sediment input consists of the mutual dilution between detrital and calcareous biogenic material. The peak detrital contribution (represented by the concentration of Al in Figure 3) occurs immediately before ORG1 coincident with the most negative $\delta^{13}C_{org}$. At the same time minimum $CaCO_3$ values of around 20% are recorded. As $CaCO_3$ recovers, [Al] and the $CaCO_3$ records appear to anti-correlate.

The behavior of organic carbon with respect to both lithogenic and biogenic components is more complex. The initial increase in organic carbon content occurs after the peak in detrital content of the sediment during the initial recovery of $CaCO_3$ (B, Figure 3). Following ORG1, but prior to ORG2, $CaCO_3$, TOC and [Al] all resemble conditions prior to the negative oxygen isotope excursion (C, Figure 3). During ORG2 the TOC and $CaCO_3$ records are out of phase by 180°, and detrital material is in phase representing the mutual dilution occurring (D, Figure 3).

3.4.2. Paleo-oxygenation

Paleo-oxygenation proxies, such as U, U/Th, V/Cr, and Ni/Co, have been used to determine water column oxygenation conditions through large periods of geological time from Quaternary sapropels [*Thomson et al.*, 1995], Jurassic mudstones [*Jones and Manning*, 1994] to the Cambrian [*Powell et al.*, 2003]. U measurements within both ORG1 and ORG2 are on average around 3 ppm, with occasional increases to 5 ppm, with background values of near zero. Ni/Co ratios are greater than 5, while V/Cr and U/Th are less than 2 and 0.75 respectively. V/Cr does, however, increase during ORG1 and ORG2 (Figure 3) from around 1 to a maximum of 1.4. Mn/Al profiles generated through the section show significant decreases during both ORG1 and ORG2 with spikes immediately following the decrease in TOC concentration (Figure 3).

A qualitative increase in the amount of pyrite is observed from the analysis of the organic residues and from the ≥ 63 μm residue foraminiferal analyses within both ORG intervals. S values are on average 0.05% of the bulk sediment but rise to greater than 1% at times in the organic rich intervals (Figure 3). These increases in concentration are coincident with peaks in TOC and the maximum negative excursions recorded in $\delta^{13}C_{org}$. Similarly Fe/Al shows a small relative increase during these intervals. Principal component analysis of the geochemical data set (Figure S3) indicates that both Fe and S are important constituents of the sediment within ORG 1 and 2 and correlate with the observed increase in pyrite and measured TOC.

The non-biological elements, (e.g. Cr, U, V) all show relatively small increases in elemental ratios during the high organic intervals, associated with the peaks in S content (Figure S4). However, they do not show the large enrichments as seen in present day anoxic environments such as the Black Sea, or in previous ocean anoxic events. The biogenic metals Zn, Ni and Cu show small (2 fold) enrichment on background values (~ 4 fold on average shale values) coincident with high TOC values and elevated S concentrations in the sediment (Figures 3, S4).

4. Discussion

4.1. Comparison to other MECO records

Our records from Alano document a perturbation to the Earth's climate system that interrupted the long term cooling of the Eocene. Previous δ^{13}C isotopic studies, both bulk and benthic foraminifera, are presented alongside the bulk δ^{13}C signal from the Alano section (Figure 4). The Alano data are plotted using the age model constructed in section 3.1 and appear to indicate an $\sim$ 100 kyr older offset for the maximum negative isotope excursion. Using carbon isotope stratigraphy the salient features of the carbon isotope record at Alano can be correlated to other global sections (tie points A-E (Figure 4). Additionally by comparing the occurrence of key biostratigraphic datums, in particular the calcareous planktonic foraminifer P13 marker species *O. beckmanni*, as well as the calcareous nannofossils *Discoaster bisectus* and *Sphenolithus furcatolithoides* a clear case can be made to correlate the isotope perturbations recorded at Alano with the previously documented MECO event [*Bohaty and Zachos*, 2003; *Bohaty et al.*, 2009]. We suggest that the uncertainity in the placement of the base of the magnetochron 18n.2n. boundary means that, within error of the age model, that the maximum δ^{13}C negative isotope excursion (labelled B, Figure 4, S5) is correlatable across the global suite of sites plotted in Figure 4 (a full discussion of this is given in the supplementary information). Furthermore, both bulk and foraminiferal records show a positive δ^{13}C excursion of up to 1.2‰ immediately after the maximum negative excursion and occurring within 50 – 150 kyrs.

Within the central-western Tethys our record from Alano shows a strong isotopic correlation with other deep ocean records, which cannot be seen in the Contessa section (Figure 4). The previous identification of MECO for the Contessa section was associated with the positive $\delta^{13}C$ excursion by *Jovane et al.* [2007]. This excursion can be re-interpreted with respect to the new Alano correlation to represent the positive $\delta^{13}C$ excursion immediately after the event (B as marked in Figure 3).

Interestingly, the gradual excursion to minimum $\delta^{13}C$ values seen at Alano is mirrored by similar patterns at ODP Site 1051 and 1263 and DSDP Site 523 (Figure 4). However, it is not recorded in the fine fraction at S. Ocean sites or in the benthic foraminiferal values from there. There a number of reasons that may account for these observed differences, including diagenetic histories, and at Alano oxidation of organic matter in the near shore environment and continental input of organic rich material to surface waters.

The other prominent features of the Alano record, the positive $\delta^{13}C$ excursion associated with ORG 2, and the intervening large negative $\delta^{13}C$ excursion, are not as well defined in the other records. We suggest that small negative excursions at ODP Sites 702, 738 and 748 at $\sim$ 39.7 Ma (labeled D+E Figure 4), and at ODP Sites 1051 and 1263 at 39.8 Ma may also be recording these two other features.

4.2. Organic Carbon Burial and Low Oxygenation of Bottom Waters

Post–MECO conditions have different lithological expressions between the central Tethyan record and the MECO event documented in the Southern Ocean, Blake Nose and other deep ocean sites. Mn is frequently used as an indicator of the sediment water interface oxygenation conditions since it precipitates as oxy-hydroxides within the range of Eh and pH values of well oxidised seawater. If the dissolved O_2 concentration decreases then the solubility of oxy-hydroxides increases and Mn^{2+} is reductively leached from the sediment under sub-oxic to anoxic conditions [*Dickens and Owen*, 1994]. Previous work on depth profiles showed that Mn^{2+} displayed this behavior in modern day oxygen minimum zones [*Klinkhammer*, 1980; *Saager et al.*, 1989] when [O_2] dropped below $\sim$ 2ml/L. In general the increased Mn^{2+} concentration comes from dissolution of Mn^{2+} phases in situ within the sediment. Minima in Mn/Al correlate with increased preservation of organic material and also pyrite occurrence, high sulphur contents, together with locally clay rich and laminated layers. Together these suggest the bottom water and pore water environment became O_2 depleted. Proxies for paleo-oxygenation conditions, such as [U], V/Cr, and Ni/Co give a mixed interpretation of the bottom water environment. Two values for the concentration of U at the oxic – dysoxic boundary in seawater have previously been suggested; 5 ppm [*Jones and Manning*, 1994] and 2 ppm [*Wignall and Ruffel*, 1990]. The Alano ORG intervals record values between these two (Figure 3) and suggests that the low O_2 conditions existed. Further evidence comes from the paleoecology of benthic foraminifera within ORG1 and ORG2. Increases in the abundance of *Uvigerina*, a taxon common in O_2 depleted, organically enriched settings [*Gooday*, 2003] together with increases in other biserial and triserial taxon (e.g. bolivinids) and the species *Hanzawaia ammophila* are recorded. This latter taxa has been reported in high abundances in Ypresian sapropels of the Peri-Tethys and has been interpreted as an indicator of dysoxic conditions [*Oberhänsli*, 2000]. Different values from less than 2 to 0.3 ml/l have been placed on the bottom O_2 conditions indicated by these taxa [*Tyson and Pearson*, 1991; *Kaiho*, 1994] and this agrees well with the O_2 constraint from the observed Mn front. Furthermore, the spikes in Mn/Al immediately preceeding both ORG1 and ORG2, indicate good correlation between re-oxygenation of pore waters and a decrease in organic carbon preservation. The offset between the TOC record marking the end of ORG1 and the inorganic bulk carbonate δ^{13}C record indicates that preservation of organic carbon in ORG1 was probably affected by burn down of the organic material after deposition. ORG2 is not similarly affected but the rapid change in lithology described at the top of this bed is indicative of a hiatus removing an unknown amount of material and time.

At the present day, terrestrial organic matter has a more negative δ^{13}C signal than marine organic matter and the negative $\delta^{13}C_{org}$ excursions during the burial of ORG1 and ORG2 therefore suggest an increased delivery of terrestrial organic matter to the sediment. This would suggest that increased terrestrial material would provide increased nutrients to the sea surface and increase productivity. This interpretation is consistent with calcareous nannofossil assemblage changes from oligotrophic to euthrophic taxa [*Agnini et al.*, 2007b] which suggest a high food high productivity ocean. At the same time minima in the $\leq 63\mu$m size fraction (not shown) suggests a shift to more chemical weathering indicative of wetter more humid environments, or a shift in palaeocoastal position to deeper waters.

Increases in the relative proportion of detrital material are synchronous with the maximum negative isotope conditions and the $\delta^{13}C_{org}$ excursion suggesting that terrestrially derived nutrients, rather than upwelling, was a source to feed this productivity increase. Further evidence for terrestrial input comes from the preservation of spores, pollen and wood identified in the organic residues. The increase in nutrients prior to the MECO peak suggests that an increase in rain rate of organic material would lead to increased O_2 utilization in bottom waters and in the sediment leading to a dysoxic bottom water environment and more reducing conditions in the sediment allowing the formation of pyrite and the increased solubility of Mn^{2+}. Small increases in the sulphide fixed trace elements (Figure S4) suggest that anoxia was reached neither in the sediment nor the water column for any extended period of time.

Several potential mechanisms could have caused the low oxygenation conditions. An increase in nutrients would lead to an increase in productivity in surface waters and sediment rain to bottom waters where increased O_2 utilization in the decomposition of organic matter would lead to the generation of dysoxic water conditions. Secondly changes in bottom water temperatures, if present, may act to decrease the solubility of O_2 in the waters and promote dysoxia. A third alternative mechanisms could involve the upwelling of a low O_2 water upwelled from depth bathing the site as suggested for black shale formation during the PETM in the eastern Tethys [*Speijer and Morsi*, 2002]. Fourthly, more sluggish ocean circulation driven by possible increases in ocean temperature (e.g. *Bohaty et al.* [2009] would have decreased the rate at which O_2 poor waters were replaced.

The productivity driven mechanism for ORG burial, similar to OAE2 of the Cretaceous [*Schlanger and Jenkyns*, 1976], would likely be coupled with an increase in sedimentation rate during this interval, both from increased terrestrial input and in increases in productivity of calcareous organisms, which are seen to shift towards euthrophic taxa [*Agnini et al.*, 2007a; *Luciani et al.*, 2009]. Similar increases in sedimentation rate are seen in expanded PETM sections in the Belluno Basin [*Giusberti et al.*, 2007] and other marginal marine sections [*Sluijs et al.*, 2008b]. However, the age model presented in section 3.1 maintains a constant linear sedimentation rate across these intervals. The placement of magnetochron C18n.2r (supplementary information) is poorly constrained, however, it tentatively suggests sedimentation rates up to 6 times faster during the ORG2 interval, consistent with the productivity hypothesis. Together with an increased sedimentation rate the combination of increased burial rate of organic carbon, and the decreased [O_2] resulted in increased preservation of organic carbon within the sediment. Variations in the amount of TOC preserved in ORG2 appear cyclic and suggest a strong orbital control on the preservation of organic carbon. This increase in LSR results in cycle spacing of $\sim$ 17 kyrs during ORG 2. Reduced preservation could therefore be related to either increased O_2 in bottom waters or reduction in productivity in the surface waters driven by orbital variations in run off.

During the PETM warming soil and atmospheric moisture increased in the northern mid-latitudes [*Bowen et al.*, 2004], and there was enhanced continental weathering around the Tethyan regions [*Bolle and Adatte*, 2001]. Increased humidity, fluvial run-off and a strengthening of the hydrological cycle was also seen in the Arctic Ocean [*Sluijs et al.*, 2006; *Pagani et al.*, 2006]. If these responses to global warming at the PETM are considered to be analogous to expected responses to warming during MECO then the fluctuations in TOC may relate to orbital (precessional) driven changes in weathering and fluvial input.

Similarly, warmer temperatures may have slowed the rate of ocean circulation. The combination of a slower circulation, high nutrient input and possible fresh water lid to the Tethys could have led to ocean stratification and driven the low O_2 conditions at this site promoting organic carbon burial and preservation.

5. Mechanisms of global change

The organic carbon burial following the maximum negative carbon isotope excursion is the first documented for MECO at any of the globally distributed sites. This may in part be related to the very different geographic location occupied by Alano compared to the deep ocean sites reported by *Bohaty et al.* [2009] or the oxidation of organic carbon in the deep ocean. The organic carbon burial recorded here allows us to briefly speculate on the recovery of this transient warming event.

5.1. Recovery to the general cooling trend

The two main mechanisms for drawing down pCO_2 are, (1) increased burial of organic burial and (2) increased weathering of silicate rocks. Both operate on significantly different timescales (kyrs and Myrs respectively). Deep sea benthic δ^{18}O records from the Southern Ocean (Figure 4) [*Bohaty and Zachos*, 2003; *Bohaty et al.*, 2009] show a rapid recovery to pre-warming values on timescales of less than 100kyrs. Globally the increased δ^{13}C values both at Alano and from other records distributed globally (Figure 1) suggest an increase in the the rate of organic burial relative to total carbon burial, although a number of assumptions have to be made for this interpretation of the δ^{13}C record [*Kump and Arthur*, 1999]. The record at Alano, bears close similarities to Cretaceous records of ocean anoxic events [*Schlanger and Jenkyns*, 1976] where δ^{13}C records a geologically instantaneous very rapid shift to higher values, associated with large burial of organic carbon and for OAE 2 a productivity driven cause of anoxia.

The initial increases in detrital material and $\delta^{13}C_{org}$ recorded at Alano prior to the acme of the negative δ^{13}C excursion suggest that the nutrient driven increase in productivity and subsequent increased utilization and storage began prior to this point, but only had an effect when either the source of $p\mathrm{CO}_2$ was switched off, or the preservation of organic material became greater than the $p\mathrm{CO}_2$ input. The high TOC values at the Alano section suggest that burial of organic carbon could provide a major sink for pCO_2 after warming and rapidly lower atmospheric pCO_2. Further evidence for organic carbon burial being a probable pCO_2 sink comes from deepening of the CCD over 10^4 yrs immediately following peak warming [*Bohaty et al.*, 2009] and increased mass accumulation rates of organic carbon at ODP Site 1218 [*Lyle and Lyle*, 2006]. Alternatively, weathering of terrestrial CaCO_3 [*Ridgwell and Hargreaves*, 2007] has been suggested for the recovery of the CCD at the ETM2 [*Stap et al.*, 2009] and could potentially negate the need for organic carbon burial.

The enhanced preservation and burial of organic carbon was driven by both a decrease in bottom water oxygenation conditions and an increase in nutrient supply to surface waters at Alano. Previous records of MECO come from deep-sea sites with little evidence of increased carbon burial, although Site 1218 in the equatorial Pacific records an increase in organic carbon accumulation rates [*Lyle and Lyle*, 2006; *Lyle et al.*, 2008]. However, if burial was mainly restricted to marginal and continental shelf sites, as 90% of present day organic burial is [*Hedges and Keil*, 1995], then as yet these records will not have been discovered and further sections remain to be studied to confirm or reject this hypothesis.

5.2. Removal of organic carbon from the atmosphere

Average TOC values are give in table 1 and show an order of magnitude increase in ORG1 and ORG2 compared to the pre-CIE and post event. Could this burial of organic carbon be sufficient to cause the positive carbon isotope excursions seen following the maximum negative δ^{18}O and δ^{13}C excursions? How much carbon could be removed from the ocean-atmosphere system through accelerated organic carbon burial?

If we assume that TOC values both before the maximum negative δ^{13}C excursion (A), Figure 3, and post recovery (E) represent the average TOC burial during the Eocene, it becomes clear that there was excess carbon burial during the MECO recovery period. However, trying to extrapolate these numbers to determine total carbon burial is not simple, even allowing the assumption that Alano represents global conditions on shelves post peak MECO. Furthermore, present day attempts to estimate carbon fluxes to / from the global ocean and coastal areas has proved difficult [*Borges*, 2005] and organic flux to the sea floor is very dependent on local and regional conditions creating a heterogeneous coastal ocean. It is possible though, to make some first order calculations to test the possible organic carbon burial mechanism for the recovery from the MECO event. Today, the coastal shelf area is some 26 x10^6 km2 [*Walsh*, 1991], which is estimated to be $\sim$ 50 - 75 % of the Eocene coastal shelf area [*John et al.*, 2008], when sea-levels were up to and above 100m higher than the present day [*Miller et al.*, 2005]. We consider that our estimate of TOC averaged for intervals A+E (Figure 3) represent background organic carbon sedimentation at this time and therefore the total extra organic carbon burial during ORG1 can be calculated. We assume for this calculation that LSR remained constant and we consider two possible end member dry bulk densities (0.5 and 1 g/cm^3) to calculate mass accumulation rates. Extrapolated to the whole of the present coastal area this would bury an additional 542 to 872 GT of carbon during ORG1 and 1160 to

1656 GT during ORG2. These values are similar to estimates of organic carbon burial on continental settings during the PETM [*John et al.*, 2008] and only slightly less than estimates of carbon released at the PETM: 1500 – 2200 GT C [*Dickens et al.*, 1997] and 4500 GT C [*Zachos et al.*, 2005].

Using our estimate from the first order calculation we apply the increased organic carbon burial over the period of ORG1 to the simple steady state carbon cycle system described by *Kump and Arthur* [1999]. After applying the increased burial to the system we estimate that for the volumes of organic carbon buried above a 0.57‰ positive isotope excursion should be recorded in the global ocean. Compared to benthic records from the Southern Ocean [*Bohaty et al.*, 2009], this shift accounts for only about two–thirds of the measured δ^{13}C positive shift occurring in the first 50 – 100,000 years after the peak of the event.

Two possibilities arise from this observation. 1) That Alano is not a typical section, it is slightly deeper than true coastal sections and the amount of organic carbon buried may well have been higher. Burndown of TOC in ORG 1 is likley to have occurred. Similarly, if Eocene shelf areas estimates are used this will again increase the estimate by a factor of 1.5 – 2. 2) That increases in $CaCO_3$ mass accumulation rates as seen following the event [*Bohaty et al.*, 2009] and also hypothesised by *Ridgwell and Zeebe* [2005] at the PETM and shown by *Stap et al.* [2009] for the Eocene thermal maximum 2 (ETM2) and H2 event may explain the rest of the recovery. Previously, silicate weathering was the foremost mechanism for the deepening of the lysocline during the recovery of the PETM [*Dickens et al.*, 1997; *Ravizza et al.*, 2001; *Kelly et al.*, 2005; *Zachos et al.*, 2005]. However, on timescales less than 100 kyrs this mechanism is suggested to be relatively ineffective [*Ridgwell and Zeebe*, 2005]. On shorter timescales ($\leq$ 20 kyrs) neutralization of the increased pCO_2 in the atmosphere is predicted to occur via weathering of carbonates in soils and exposed surfaces thereby increasing the ocean [HCO_3^-] and deepening the lysocline [*Archer et al.*, 1998; *Ridgwell and Zeebe*, 2005]. The weathered [HCO_3^-] would have a more positive $\delta^{13}C$ signal that the exogenic carbon reservoir at the time and would therefore help drive a recovery in the depth of the lysocline and a positive shift in the $\delta^{13}C$ value.

We suggest that together, increased organic carbon burial during the recovery phase and increases in the accumulation of $CaCO_3$ in sections above the lysocline, as seen in the records of *John et al.* [2008] for shallow New Jersey margin sections at the PETM and increases in the mass accumulation rates seen at DSDP Site 523 in the S. Atlantic [*Bohaty et al.*, 2009], explain the rapid positive increase in the $\delta^{13}C$ at MECO immediately after the maximum negative $\delta^{13}C$ excursion. Until further shallow coastal sections for the MECO event are identified the organic carbon scenario remains one hypothesis, which requires further study.

6. Conclusions

In this study middle Eocene warming is recorded in the northern hemisphere synchronously with previous records from the Southern Ocean [*Bohaty and Zachos*, 2003]. High organic carbon burial and local depleted O_2 bottom water conditions may be a local response to this warming or could potentially represent a well preserved global signal. Organic carbon burial coincident with a positive $\delta^{13}C$ excursion at Alano has been stratigraphically correlated to the Southern Ocean. We suggest high burial rates of organic carbon in marine shelf settings over kyr timescales that are consistent with global cooling recorded at Southern Ocean sites and offer the most likely mechanism for driving a pCO_2 decrease following the event. Future modeling studies may help to increase our understanding of this event.

Acknowledgments. We are grateful for the staff at Padova University, Italy who originally sampled and logged this section. DJAS thanks Professor John Marshall for help with the organic material, Professor Ian Croudace for help and advice with sediment geochemistry, and Kirsty Edgar and Steve Bohaty for numerous discussions on MECO both at Alano and elsewhere. Appy Slujis and an anonymous reviewer greatly improved this manuscript. Financial support was provided to DJAS by NERC studentship (Ref. NER/S/A/2005/13474) and to HP by grants PP/D002176/1 and PPARC/STFC and NERC grant NE/D000393/1

References

Agnini, C., E. Fornaciari, D. Rio, F. Tateo, J. Backman, and L. Giusberti (2007a), Responses of calcareous nannofossil assemblages, mineralogy and geochemistry to the environmental perturbations across the Paleocene/Eocene boundary in the Venetian Pre-Alps, *Marine Micropaleontology*, *63*, 19–38.

Agnini, C., D. J. A. Spofforth, E. Fornaciari, L. Giusberti, L. Lanci, V. Luciani, G. Muttoni, P. Grandesso, and D. Rio (2007b), Is the Middle Eocene Climatic Optimum (MECO) recorded in the central-western Tethys?, *Eos Trans. AGU*, *88(52) Fall Meet. Suppl*(52. Fall Meet. Suppl), Abstract OS11A–0188.

Agnini, C., et al. ((in press) 2009), Integrated Bio-magnetostratigaphy of the Alano di Piave section (NE Italy): A proposal and definition of the middle–late Eocene boundary, *GSA Bulletin*.

Archer, D., H. Kheshgi, and E. Maier-Reimer (1998), Dynamics of fossil fuel co_2 neutralization by marine $caco_3$, *Global Biogeochemical Cycles*, *12*(2), 259–276.

Berggren, W. A., and P. N. Pearson (2005), A revised tropical to subtropical paleogene planktonic foraminiferal zonation, *Journal of Foraminiferal Research*, *35*(4), 279–298.

Berggren, W. A., D. V. Kent, C. C. Swisher, and M.-P. Aubry (1995), A revised Cenozoic geochronology and chronostratigraphy, in *Geochronology, time scales and global stratigraphic correlation (SEPM Special Publication)*, vol. 54, edited by B. W. A., D. V. Kent, M.-P. Aubry, and J. Hardenbol, pp. 129–212, Society for Sedimentary Geology (SEPM).

Berner, R., and Z. Kothavala (2001), GEOCARB III: A revised model of atmospheric CO_2 over phanerozoic time, *American Journal of Science*, *301*(2), 182–204.

Bohaty, S. M., and J. C. Zachos (2003), Significant Southern Ocean warming event in the late middle Eocene, *Geology*, *31*(11), 1017–1020.

Bohaty, S. M., J. C. Zachos, F. Florindo, and M. L. Delaney (2009), Coupled greenhouse warming and deep-sea acidification in the middle Eocene, *Paleoceanography*, *24*, doi:ARTNPA2207.

Bolle, M. P., and T. Adatte (2001), Palaeocene early Eocene climatic evolution in the Tethyan realm: clay mineral evidence, *Clay Minerals*, *36*(2), 249–261.

Borges, A. V. (2005), Do we have enough pieces of the jigsaw to integrate CO_2 fluxes in the coastal ocean?, *Estuaries*, *28*(1), 3–27.

Bosellini, F. R., and C. A. Papazzoni (2003), Palaeoecological significance of coral-encrusting foraminiferan associations: A case-study from the Upper Eocene of northern Italy, *Acta Palaeontologica Polonica*, *48*(2), 279–292.

Bowen, G. J., D. J. Beerling, P. L. Koch, J. C. Zachos, and T. Quattlebaum (2004), A humid climate state during the Palaeocene/Eocene thermal maximum, *Nature*, *432*(7016), 495–499.

Cande, S. C., and D. V. Kent (1995), Revised Calibration of the Geomagnetic Polarity Timescale for the Late Cretaceous and Cenozoic, *Journal of Geophysical Research-Solid Earth*, *100*(B4), 6093–6095.

Coxall, H. K., P. A. Wilson, H. Palike, C. H. Lear, and J. Backman (2005), Rapid stepwise onset of Antarctic glaciation and deeper calcite compensation in the Pacific Ocean, *Nature*, *433*(7021), 53–57.

Cramer, B. S., J. D. Wright, D. V. Kent, and M. P. Aubry (2003), Orbital climate forcing of delta c-13 excursions in the late paleocene-early eocene (chrons c24n-c25n), *Paleoceanography*, *18*(4).

DeConto, R. M., and D. Pollard (2003), Rapid Cenozoic glaciation of Antarctica induced by declining atmospheric CO_2, *Nature*, *421*(6920), 245–249.

DeConto, R. M., D. Pollard, P. A. Wilson, H. Palike, Lear, and M. Pagani (2008), Thresholds for Cenozoic bipolar glaciation, *Nature*, *455*, 652–656.

Dercourt, J., L. E. Ricou, and B. Vrielynck (1993), *Atlas of Tethys Palaeoenvironmental Maps*, Gauthier-Villars.

Dickens, G. R., and R. Owen (1994), Late Miocene-early Pliocene manganese redirection in the central Indian-Ocean - expansion of the intermediate water oxygen minimum zone, *Paleoceanography*, *9*(1), 169–181.

Dickens, G. R., J. R. Oneil, D. K. Rea, and R. M. Owen (1995), Dissociation of oceanic methane hydrate as a cause of the carbon-isotope excursion at the end of the Paleocene, *Paleoceanography*, *10*(6), 965–971.

Dickens, G. R., M. M. Castillo, and J. C. G. Walker (1997), A blast of gas in the latest peleocene: Simulating first-order effects of massive dissociation of oceanic methane hydrate, *Geology*, *25*(3), 259–262, doi:10.1130/0091-7613(1997)025⟨0259:ABOGIT⟩2.3.CO;2.

Edgar, K. M., P. Sexton, R. Norris, P. Wilson, and S. Gibbs (2007a), Evolutionary Response of Planktic Foraminifera to a Pronounced Global Warming Event 40 Myr ago, *Eos Trans. AGU*, *88(52), Fall Meet. Suppl*(52, Fall Meet. Suppl), Abstract OS14A–03.

Edgar, K. M., P. A. Wilson, P. F. Sexton, and Y. Suganuma (2007b), No extreme bipolar glaciation during the main Eocene calcite compensation shift, *Nature*, *448*, 908–911, doi:10.1038/nature06053.

Giusberti, L., D. Rio, C. Agnini, J. Backman, E. Fornaciari, F. Tateo, and M. Oddone (2007), Mode and tempo of the Paleocene-Eocene thermal maximum in an expanded section from the Venetian pre-Alps, *Geological Society of America Bulletin*, *119*, 391–412.

Gooday, A. J. (2003), Beyond methane: Towards a theory for the Paleocene-Eocene Thermal Maximum Benthic foraminifera (protista) as tools in deep-water palaeoceanography: Environmental influences on faunal characteristics, *Advances In Marine Biology, Vol 46*, *46*, 1–90.

Hay, W. W., et al. (1999), Alternative Global Cretaceous Paleogeography, in *The Evolution of Cretaceous Ocean/Climate Systems*, vol. 332, edited by E. Barrera and C. Johnson, pp. 1–47, Geological Soceity of America Special Paper.

Hedges, J. I., and R. G. Keil (1995), Sedimentary organic-matter preservation - an assessment and speculative synthesis, *Marine Chemistry*, *49*(2-3), 81–115.

Ivany, L. C., K. C. Lohmann, F. Hasiuk, D. B. Blake, A. Glass, R. B. Aronson, and R. M. Moody (2008), Eocene climate record of a high southern latitude continental shelf: Seymour Island, Antarctica, *Geological Society of America Bulletin*, *120* (5-6), 659–678.

John, C. M., S. M. Bohaty, J. C. Zachos, A. Sluijs, S. Gibbs, H. Brinkhuis, and T. J. Bralower (2008), North American continental margin records of the Paleocene-Eocene thermal maximum: Implications for global carbon and hydrological cycling, *Paleoceanography*, *23* (2), doi:ARTNPA2217.

Jones, B., and D. Manning (1994), Comparison of geochemical indexes used for the interpretation of palaeoredox conditions in ancient mudstones, *Chemical Geology*, *111* (1-4), 111–129.

Jovane, L., F. Florindo, R. Coccioni, J. Dinarès-Turell, A. Marsili, S. Monechi, A. P. Roberts, and M. Sprovieri (2007), The middle Eocene climatic optimum event in the Contessa Highway section, Umbrian Apennines, Italy, *Geological Society of America Bulletin*, *119* (3), 413–427.

Kaiho, K. (1994), Benthic foraminiferal dissolved-oxygen index and dissolved-oxygen levels in the modern ocean, *Geology*, *22* (8), 719–722.

Kelly, D. C., J. C. Zachos, T. J. Bralower, and S. A. Schellenberg (2005), Enhanced terrestrial weathering/runoff and surface ocean carbonate production during the recovery stages of the Paleocene-Eocene thermal maximum, *Paleoceanography*, *20* (4), pA4023.

Kennett, J. P., and L. D. Stott (1991), Abrupt deep-sea warming, palaeoceanographic changes and benthic extinctions at the end of the Paleocene, *Nature*, *353* (6341), 225–229.

Klinkhammer, G. P. (1980), Early diagenesis in sediments from the eastern equatorial Pacific 2. Pore water metal results, *Earth and Planetary Science Letters*, *49* (1), 81–101.

Kump, L. R., and M. A. Arthur (1999), Interpreting carbon-isotope excursions: carbonates and organic matter, *Chemical Geology*, *161* (1-3), 181–198.

Lear, C. H., T. R. Bailey, P. N. Pearson, H. K. Coxall, and Y. Rosenthal (2008), Cooling and ice growth across the Eocene-Oligocene transition, *Geology*, *36* (3), 251–254.

Liu, Z., M. Pagani, D. Zinniker, R. DeConto, M. Huber, H. Brinkhuis, S. R. Shah, R. M. Leckie, and A. Pearson (2009), Global Cooling During the Eocene-Oligocene Climate Transition, *Science*, *323* (5918), 1187–1190, doi:DOI10.1126/science.1166368.

Lourens, L. J., A. Sluijs, D. Kroon, J. C. Zachos, E. Thomas, U. Rohl, J. Bowles, and I. Raffi (2005), Astronomical pacing of late Palaeocene to early Eocene global warming events, *Nature*, *435* (7045), 1083–1087.

Luciani, V., C. Agnini, E. Fornaciari, L. Giusberti, D. Rio, D. Spofforth, and H. Palike (2009), Ecological and evolutionary response of Tethyan planktonic foraminifera to the Middle Eocene Climatic Optimum (Alano di Piave section, NE Italy), *Geophysical Research Abstracts*, *11* (EGU2009-10464-2).

Lyle, A. O., and M. W. Lyle (2006), Missing organic carbon in Eocene marine sediments: Is metabolism the biological feedback that maintains end-member climates?, *Paleoceanography*, *21* (2), pA2007.

Lyle, M., J. Barron, T. J. Bralower, M. Huber, A. O. Lyle, A. C. Ravelo, D. K. Rea, and P. A. Wilson (2008), Pacific ocean and Cenozoic evolution of climate, *Reviews of Geophysics*, *46* (2).

Martini, E. (1971), Standard Tertiary and Quaternary calcareous nannoplankton zonation, in *2nd Planktonic Conference*, vol. 2, edited by A. Farinacci, pp. 739–785, Tecnoscienza, Roma.

Miller, K. G., et al. (2005), The phanerozoic record of global sea-level change, *Science*, *310* (5752), 1293–1298, doi:DOI10.1126/science.1116412.

Nicolo, M. J., G. R. Dickens, C. J. Hollis, and J. C. Zachos (2007), Multiple early Eocene hyperthermals: Their sedimentary expression on the New Zealand continental margin and in the deep sea, *Geology*, *35* (8), 699–702.

Oberhänsli, V. N., Hand Beniamovskii (2000), Dysoxic bottom water events in the peri-Tethys during the late Ypresian: A result of changes in the evaporation/precipitation balance in adjacent continental regions, *Gff*, *122*, 121–123.

Pagani, M., J. C. Zachos, K. H. Freeman, B. Tipple, and S. Bohaty (2005), Marked decline in atmospheric carbon dioxide concentrations during the Paleogene, *Science*, *309*(5734), 600–603.

Pagani, M., K. Caldeira, D. Archer, and J. C. Zachos (2006), An ancient carbon mystery, *Science*, *314*(5805), 1556–1557.

Pälike, H., R. D. Norris, J. O. Herrle, P. A. Wilson, H. K. Coxall, C. H. Lear, N. J. Shackleton, A. K. Tripati, and B. S. Wade (2006a), The Heartbeat of the Oligocene Climate System, *Science*, *314*(5807), 1894–1898, doi:10.1126/science.1133822.

Powell, W. G., P. A. Johnston, and C. J. Collom (2003), Geochemical evidence for oxygenated bottom waters during deposition of fossiliferous strata of the Burgess Shale Formation, *Palaeogeography Palaeoclimatology Palaeoecology*, *201*(3-4), 249–268, doi:DOI10.1016/S0031-0182(03)00612-6.

Ravizza, G., R. D. Norris, J. Blusztajn, and M.-P. Aubry (2001), An osmium isotope excursion associated with the late Paleocene thermal maximum: Evidence of intensified chemical weathering, *Paleoceanography*, *16*(2), 155–163.

Raymo, M. E. (1991), Geochemical evidence supporting Chamberlin,T.,C. theory of glaciation, *Geology*, *19*(4), 344–347.

Rea, D. K., and M. W. Lyle (2005), Paleogene calcite compensation depth in the eastern subtropical Pacific: Answers and questions, *Paleoceanography*, *20*(1), doi:ARTNPA1012.

Ridgwell, A., and J. C. Hargreaves (2007), Regulation of atmospheric CO2 by deep-sea sediments in an Earth system model, *Global Biogeochemical Cycles*, *21*(2), doi:ARTNGB2008.

Ridgwell, A., and R. E. Zeebe (2005), The role of the global carbonate cycle in the regulation and evolution of the earth system, *Earth and Planetary Science Letters*, *234*(3-4), 299–315.

Saager, P. M., H. J. W. Debaar, and P. H. Burkill (1989), Manganese and iron in Indian-Ocean waters, *Geochimica Et Cosmochimica Acta*, *53*(9), 2259–2267.

Schlanger, S. O., and H. C. Jenkyns (1976), Cretaceous anoxic events: causes and consequences, *Geologie en Mijnbouw*, *55*, 179–184.

Scotese, C. R. (2002), http://www.scotese.com (paleomap website).

Sexton, P. F., P. A. Wilson, and R. D. Norris (2006), Testing the Cenozoic multisite composite delta O-18 and delta C-13 curves: New monospecific Eocene records from a single locality, Demerara Rise (Ocean Drilling Program Leg 207), *Paleoceanography*, *21* (2), pA2019.

Sluijs, A., U. Rohl, S. Schouten, H. J. Brumsack, F. Sangiorgi, J. S. S. Damste, and H. Brinkhuis (2008a), Arctic late Paleocene-early Eocene paleoenvironments with special emphasis on the Paleocene-Eocene thermal maximum (Lomonosov Ridge, Integrated Ocean Drilling Program Expedition 302), *Paleoceanography*, *23* (1), pA1S11.

Sluijs, A., et al. (2006), Subtropical arctic ocean temperatures during the Palaeocene/Eocene thermal maximum, *Nature*, *441* (7093), 610–613.

Sluijs, A., et al. (2008b), Eustatic variations during the Paleocene-Eocene greenhouse world, *Paleoceanography*, *23* (4), doi: ARTNPA4216.

Smith, A., D. G. Smith, and B. M. Funnell (1994), *Atlas of Mesozoic and Cenozoic Coastlines*, CUP.

Speijer, R. P., and A. M. M. Morsi (2002), Sea-level changes and black shales assoicated with the late paleocene thermal maximum: organic-gochemical and micropaleontologic evidence from the southern tethyan margin (egypt-israel), in *Geological Soceity of America Special Paper*, vol. 356, pp. 533–549.

Stap, L., A. Sluijs, E. Thomas, and L. Lourens (2009), Patterns and magnitude of deep sea carbonate dissolution during Eocene Thermal Maximum 2 and H2, Walvis Ridge, southeastern Atlantic Ocean, *Paleoceanography*, *24*, doi:ARTNPA1211.

Thomas, D. J., J. C. Zachos, T. J. Bralower, E. Thomas, and S. Bohaty (2002), Warming the fuel for the fire: Evidence for the thermal dissociation of methane hydrate during the Paleocene-Eocene thermal maximum, *Geology*, *30* (12), 1067–1070.

Thomson, J., N. C. Higgs, T. R. S. Wilson, I. W. Croudace, G. J. Delange, and P. J. M. Vansantvoort (1995), Redistribution and geochemical behavior of redox-sensitive elements around s1, the most recent eastern Mediterranean sapropel, *Geochimica Et Cosmochimica Acta*, *59* (17), 3487–3501.

Tripati, A., J. Backman, H. Elderfield, and P. Ferretti (2005), Eocene bipolar glaciation associated with global carbon cycle changes, *Nature*, *436* (7049), 341–346.

Tyson, R., and T. Pearson (1991), Modern and ancient continental shelf anoxia: an overview, in *Modern and Ancient Continental Shelf Anoxia*, vol. 58, edited by R. Tyson and T. Pearson, pp. 1–24, Geological Society Speical Publication.

Wade, B. S. (2004), Planktonic foraminiferal biostratigraphy and mechanisms in the extinction of Morozovella in the late middle Eocene, *Marine Micropaleontology*, *51* (1-2), 23–38.

Walsh, J. J. (1991), Importance of continental margins in the marine biogeochemical cycling of carbon and nitrogen, *Nature*, *350* (6313), 53–55.

Wignall, P. B., and A. H. Ruffel (1990), The influence of a sudden climatic-change on marine deposition in the Kimmeridgian of northwest Europe, *Journal of the Geological Society*, *147*, 365–371.

Zachos, J. C., T. M. Quinn, and K. A. Salamy (1996), High-resolution (10^4 years) deep-sea foraminiferal stable isotope records of the Eocene-Oligocene climate transition, *Paleoceanography*, *11* (3), 251–266.

Zachos, J. C., M. Pagani, L. Sloan, E. Thomas, and K. Billups (2001), Trends, rhythms, and aberrations in global climate 65 Ma to present, *Science*, *292* (5517 1), 686–693.

Zachos, J. C., M. W. Wara, S. Bohaty, M. L. Delaney, M. R. Petrizzo, A. Brill, T. J. Bralower, and I. Premoli-Silva (2003), A transient rise in tropical sea surface temperature during the Paleocene-Eocene Thermal Maximum, *Science*, *302* (5650), 1551–1554.

Zachos, J. C., et al. (2005), Rapid acidification of the ocean during the Paleocene-Eocene thermal maximum, *Science*, *308* (5728), 1611–1615.

Figure 1. A) Palaeogeographic reconstruction of the Lessini Shelf: 1) deep water mudstones of the surrounding Jurassic basins; 2) Palaeogene lagoon and shelf edge reefs; 3) Palaeogene pelagic claystones and marlstones (modified from *Bosellini and Papazzoni* [2003]) The approximate location of the Alano site is marked by a star. B) Paleogeographic reconstruction at 40Ma [*Hay et al.*, 1999] showing location of sites where MECO has been identified and location of Alano (A) and Contessa (C). C) Same reconstruction centered over the Tethys area. Paleoenvironmental reconstruction from *Scotese* [2002] and interpretation *Dercourt et al.* [1993]. Alano di Piave location marked by the star.

Figure 2. Bulk carbonate stable isotopes $\delta^{13}C$, δ^{18}O and percentage $CaCO_3$ over the entire Alano di Piave section. Linear sedimentation rates are calculated using magnetochron boundaries with ages from [*Cande and Kent*, 1995; *Pälike et al.*, 2006a]

Figure 3. Sediment Geochemistry across the MECO interval. From top $\delta^{13}C_{cc}$ and $\delta^{13}C_{org}$, % $CaCO_3$, Total Organic Carbon (TOC), % sulfur, Mn/Al, [Al], [U] and V/Cr. Dashed lines on U (ppm) graph represent oxic - dysoxic boundary of [*Wignall and Ruffel*, 1990] and [*Jones and Manning*, 1994] respectively. Elemental data measured on discrete XRF samples. Overlaid bands indicate organic rich intervals. Labels A – E deconstruct the $\delta^{13}C$ record into phases and are described in the results

Figure 4. Stratigraphic correlation of $\delta^{13}C_{Alano}$ to global records from *Bohaty et al.* [2009] and for Contessa from *Jovane et al.* [2007]. The FO and LO of the marker species *O.beckmanni* and S. furcatolithoides are shown for the Alano section. Records from sites as marked in the Figure and locations as seen in Figure 1. Letters A-E refer to correlation tie points between records.

Table 1. Average TOC content for sections, A, B, C, D, E as referred to in main text and Figure 3. Calculated mass accumulation rates assuming constant linear sedimentation rate and dry bulk density. As no measure of dry bulk density is available we use a value of 1g/cc. We note that the ≥ 63 μm residue is lowest during the organic rich units and therefore the expected dry bulk density here would be expected to be higher.

Section	A(Pre-CIE)	B(ORG1)	C	D(ORG2)	E(Recovery)
% TOC	0.17	1.83	0.23	1.5	0.15
MAR*	0.003	0.033	0.004	0.027	0.002

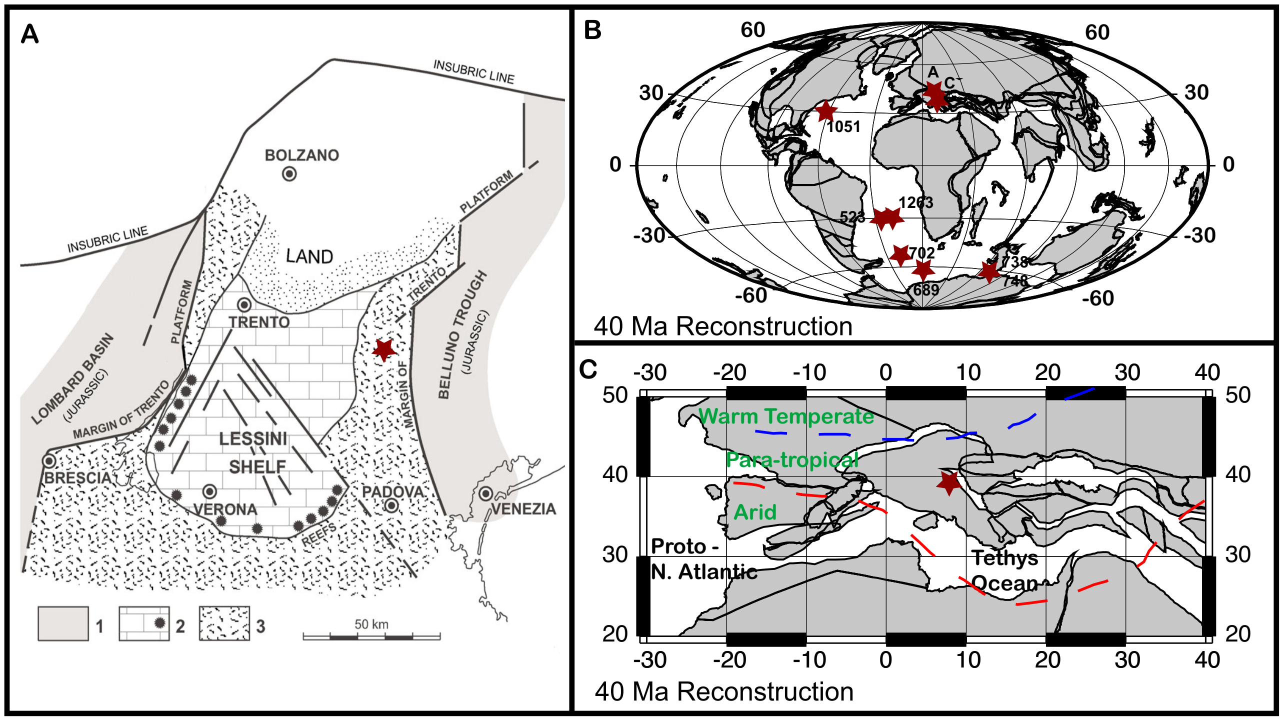

A
INSUBRIC LINE
BOLZANO
INSUBRIC LINE
PLATFORM
LAND
TRENTO
TRENTO
PLATFORM
LOMBARD BASIN
(JURASSIC)
MARGIN OF TRENTO
LESSINI
SHELF
MARGIN OF
BELLUNO TROUGH
(JURASSIC)
BRESCIA
VERONA
REEFS
PADOVA
VENEZIA
1
2
3
50 km
B
40 Ma Reconstruction
1051
1263
523
702
689
738
748
C
Warm Temperate
Para-tropical
Arid
Proto -
N. Atlantic
Tethys
Ocean
40 Ma Reconstruction

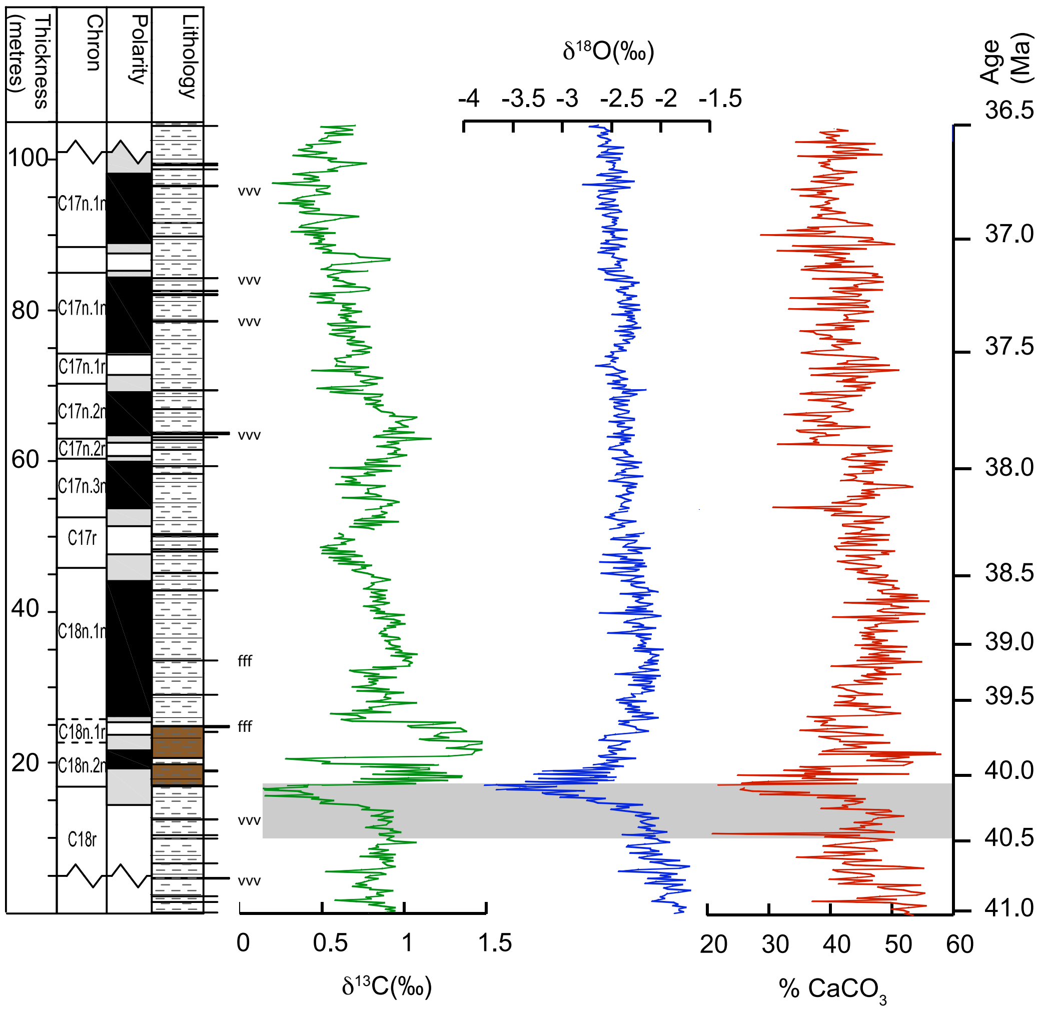

Sapropel type interval - locally clay rich and laminated
Light grey marls
Prominent bed of variable composition
vvv Crystal tuff layer > 6cm thick
fff Bioclastic layer > 6cm thick

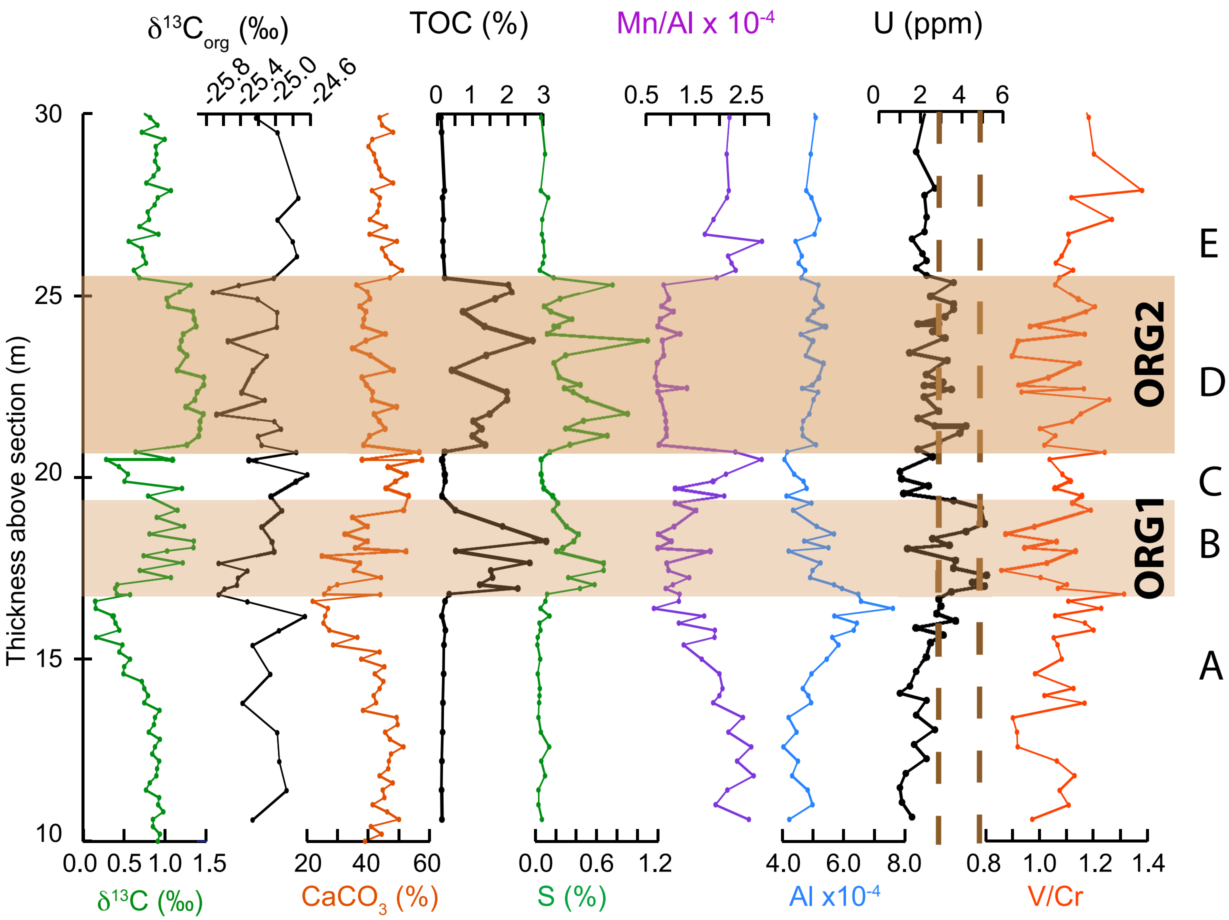

δ13Corg (‰)
-25.8
-25.4
-25.0
-24.6
TOC (%)
0 1 2 3
Mn/Al x 10-4
0.5 1.5 2.5
U (ppm)
0 2 4 6
Thickness above section (m)
30
25
20
15
10
E
ORG2
D
C
ORG1
B
A
0.0 0.5 1.0 1.5
δ13C (‰)
20 40 60
CaCO3 (%)
0.0 0.6 1.2
S (%)
4.0 6.0 8.0
Al x10-4
0.8 1.0 1.2 1.4
V/Cr

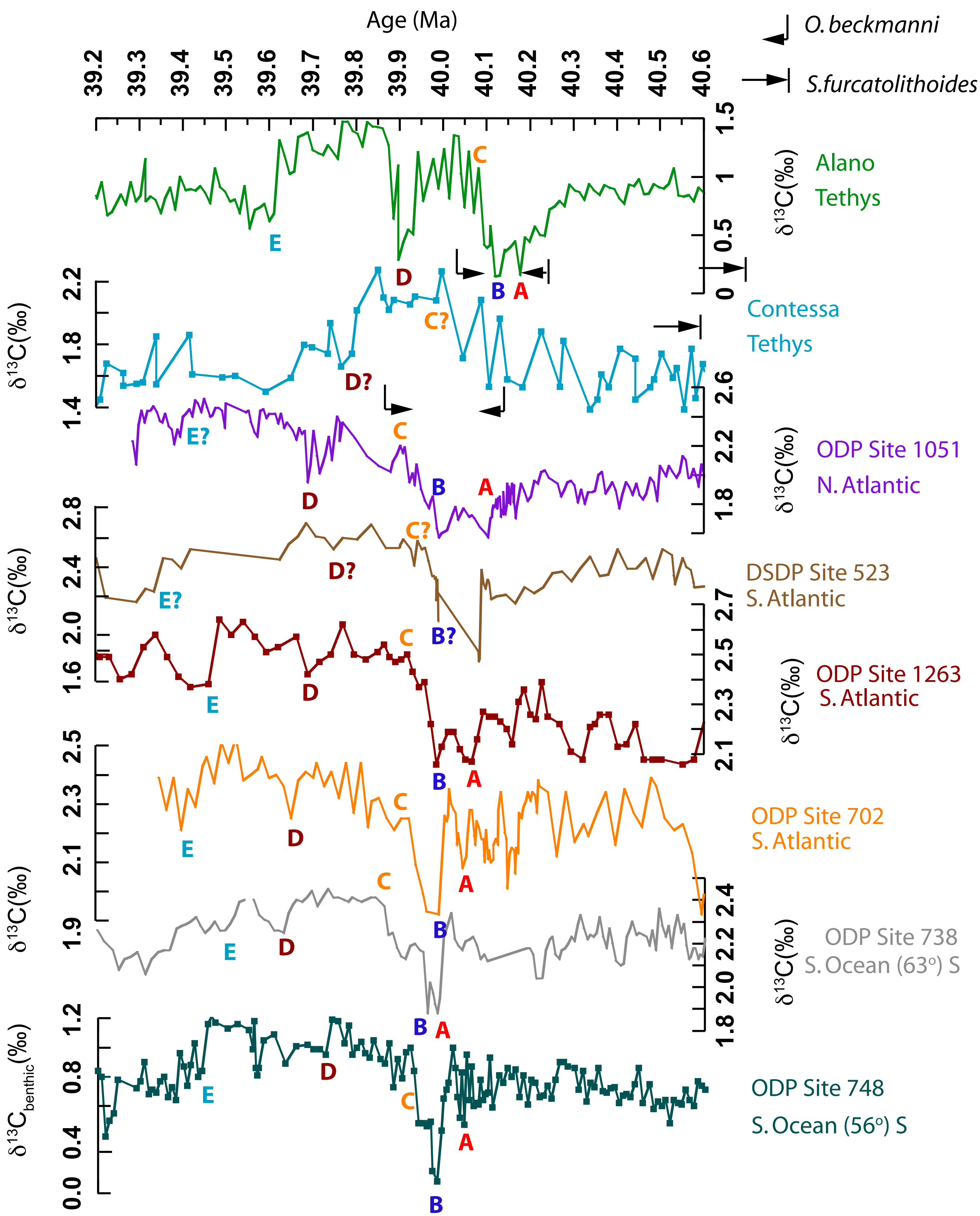
Age (Ma)
39.2
39.3
39.4
39.5
39.6
39.7
39.8
39.9
40.0
40.1
40.2
40.3
40.4
40.5
40.6
O. beckmanni
S.furcatolithoides
Alano
Tethys
Contessa
Tethys
ODP Site 1051
N. Atlantic
DSDP Site 523
S. Atlantic
ODP Site 1263
S. Atlantic
ODP Site 702
S. Atlantic
ODP Site 738
S. Ocean (63°) S
ODP Site 748
S. Ocean (56°) S
$\delta^{13}C$(‰)
$\delta^{13}C_{benthic}$(‰)
A
B
C
D
E
B?
C?
D?
E?

```
\begin{table*}
\caption{\label{tableTOC} Average TOC content for sections, A, B, C, D, E
as referred to in main text and Figure 3. Calculated mass accumulation
rates assuming constant linear sedimentation rate and dry bulk density.
As no measure of dry bulk density is available we use a value of 1g/cc.
We note that the $\ge$ 63 $\mu$m residue is lowest during the organic
rich units and therefore the expected dry bulk density here would be
expected to be higher. }
\begin{center}
\begin{tabular}{lccccc}
\hline

Section&A(Pre-CIE)&B(ORG1)&C&D(ORG2)&E(Recovery)\\
\hline
\% TOC&0.17&1.83&0.23&1.5&0.15\\
MAR*&0.003&0.033&0.004&0.027&0.002\\

\end{tabular}
\end{center}
\end{table*}
```